Journal of Materials Chemistry A

High-temperature failure behaviour and mechanism of K-based additives in Li-Mg-N-H hydrogen storage systems

Journal:	*Journal of Materials Chemistry A*
Manuscript ID:	TA-ART-01-2014-000025.R1
Article Type:	Paper
Date Submitted by the Author:	01-Mar-2014
Complete List of Authors:	Li, Chao; Zhejiang University, Department of Materials Science and Engineering Liu, Yongfeng; Zhejiang University, Department of Mateials Science and Engineering Yang, Yanjing; Zhejiang University, Department of Mateials Science and Engineering Gao, Mingxia; Zhejiang University, Department of Materials Science and Engineering Pan, Hongge; Zhejiang University, Department of Materials Science and Engineering

SCHOLARONE™
Manuscripts

Cite this: DOI: 10.1039/c0xx00000x

ARTICLE TYPE

www.rsc.org/xxxxxx

High-temperature failure behaviour and mechanism of K-based additives in Li-Mg-N-H hydrogen storage systems†

Chao Li, Yongfeng Liu,* Yanjing Yang, Mingxia Gao and Hongge Pan*

Received (in XXX, XXX) Xth XXXXXXXXX 20XX, Accepted Xth XXXXXXXXX 20XX

DOI: 10.1039/b000000x

We report the high-temperature failure behaviours and mechanisms of K-based additives in the $Mg(NH_2)_2$-2LiH hydrogen storage system. The on-set of hydrogen release from $Mg(NH_2)_2$-2LiH-0.08KF sample is approximately 80 °C; this is a 50 °C reduction in comparison with the pristine $Mg(NH_2)_2$-2LiH. However, the positive effects of K-based additives disappear when the hydrogen release and uptake of the KF-added $Mg(NH_2)_2$-2LiH samples are performed at higher temperatures (> 200 °C). The change in the crystal structure of the dehydrogenation product, the enlargement in the grain and particle sizes of the dehydrogenation/hydrogenation products, and the increase in the inhomogeneous degree of mixing and distribution of K-based additive should be the three most important reasons for the increased operating temperature during the follow-up cycles. In particular, the ability of K-based additives to lower the operating temperature for hydrogen storage in the $Mg(NH_2)_2$-2LiH system can be sufficiently recovered after ball milling. Therefore, the failure of K-based additives after high-temperature treatment is only phenomenological instead of being natural. Strictly limiting the dehydrogenation/hydrogenation of the K-added $Mg(NH_2)_2$-2LiH system at lower temperatures is critical for maintaining the superior effect of K-based additives.

Introduction

The crucial challenge opposing the large-scale use of hydrogen as an energy carrier is storage in a safe, efficient and reversible system.[1] Currently, solid-state hydrogen storage in Metal-N-H systems have been extensively investigated because Li_3N can reversibly store 11.4 wt% hydrogen using the following two-step reaction.[2]

$$Li_3N+H_2 \leftrightarrow Li_2NH+LiH \quad (1)$$

$$Li_2NH+H_2 \leftrightarrow LiNH_2+LiH \quad (2)$$

However, thermodynamic analyses have shown that the hydrogen release from $LiNH_2$-2LiH and $LiNH_2$-LiH is a highly endothermic process, and the reaction enthalpies are 80 and 66 kJ mol^{-1} of H_2, respectively.[2,3] Therefore, the operating temperature at 1 bar equilibrium pressure exceeds 250 ºC and is therefore too high for practical on-board applications. By substituting $LiNH_2$ with $Mg(NH_2)_2$, a reversible $Mg(NH_2)_2$-2LiH system was developed via reaction (3), significantly improving the thermodynamics of the hydrogen storage.[4,5]

$$2LiNH_2+MgH_2 \rightarrow Mg(NH_2)_2+2LiH \leftrightarrow Li_2MgN_2H_2+2H_2 \quad (3)$$

Approximately 5.6 wt% hydrogen can be stored reversibly in the above system. The reaction enthalpy change was calculated to be ~ 39 kJ mol^{-1} H_2,[6] making it lower than that of the $LiNH_2$-2LiH and $LiNH_2$-LiH systems. The operating temperature was ~ 90 ºC at 1 bar equilibrium pressure, satisfying the necessary requirement for proton exchange membrane fuel cells (PEMFCs).[6] Unfortunately, a reasonable rate for hydrogen release/uptake was achieved only at a temperatures up to 200 ºC due to the rather high kinetic barrier.[6,7]

To improve the hydrogen storage properties of the $Mg(NH_2)_2$-2LiH system, great effort has been devoted to optimising additives or catalysts in recent years. It was reported that the dehydrogenation/hydrogenation kinetics of $Mg(NH_2)_2$-2LiH were enhanced after adding $Li_2MgN_2H_2$, carbon nanotubes, $TiCl_3$, VCl_3, $Ti_3Cr_3V_4$, TiN, Li_3N, Ph_3PO_4, graphite-supported Ru, NaOH, $LiBH_4$, $ZrCoH_3$, $NaBH_4$, $Mg(BH_4)_2$, $Ca(BH_4)_2$ or K-based compounds.[7-26] In particular, K-based compounds exhibited superior catalytic activity in the $Mg(NH_2)_2$-2LiH system. The peak temperature for hydrogen release from the $Mg(NH_2)_2$-1.9LiH-0.1KH sample was 132 ºC, which is 54 ºC lower than that of the $Mg(NH_2)_2$-2LiH sample.[22] Reversible hydrogen storage was achieved even at temperatures as low as 107 ºC in the PCT model. In addition, our previous work also revealed that the 0.07KOH-doped $Mg(NH_2)_2$-2LiH sample could reversibly store ~ 4.92 wt% hydrogen with a starting dehydrogenation temperature of only 75 ºC and the peak temperature of 120 ºC.[25] Unfortunately, the previous investigations focused primarily on the first dehydrogenation/hydrogenation cycle at lower temperatures.[22,23,25] The long-term cycling behaviour of the K-added samples and the effects on the operating temperatures have not been investigated or discussed to date. Interestingly, we

observed that the KF-added $Mg(NH_2)_2$-2LiH system exhibited hydrogenation/dehydrogenation behaviours nearly identical to the pristine sample in the subsequent cycling when dehydrogenated above 250 °C or hydrogenated above 210 °C.[26] A similar phenomenon was also found in the KH-added $LiNH_2$-MgH_2 system and the KH-added sample cycled at 200 ºC even displayed a much slower dehydrogenation rate than that of the pristine sample after the first dehydrogenation/hydrogenation cycle.[24] Specifically, the ability of K-based additives to decrease the operating temperatures for hydrogen storage in the Li-Mg-N-H system disappears after dehydrogenation/hydrogenation at higher temperatures (> 200 °C), specifically high-temperature failure. Improved dehydrogenation properties were regained after ball milling the K-added $Mg(NH_2)_2$-2LiH samples after dehydrogenation/hydrogenation at higher temperatures.[24,26] However, in-depth investigations of the underlying mechanism of the high-temperature failure of K-based additives have not been conducted. These studies are fundamentally important for improving the hydrogen storage properties of the metal-N-H system further and developing long-term cycling hydrogen storage materials.

In this work, we used the $Mg(NH_2)_2$-2LiH-0.08KF sample described as an optimal sample reported in our previous work[26] as an example. The crystal structure, the particle/grain size of the samples and the degree of dispersion/mixing of the additives were systematically investigated and compared at various dehydrogenation/hydrogenation temperatures. The higher operating temperature triggers a structural transition in the dehydrogenation product, enlarges the grain and particle size, and decreases the degree of dispersion and mixing of the catalytic species, inducing the phenomenological failure in the catalytic activity of K-based additives. This finding provides insight into the role of the K-based additive during the dehydrogenation/hydrogenation of K-added Li-Mg-N-H systems and guides the development of reversible hydrogen storage systems with long-term cyclability for practical applications.

Experimental section

Chemicals and sample preparation

LiH (purity 98%) and KF (purity 99%) were purchased from Alfa-Aesar and Sinopharm, respectively, and used as received without further purification. KH (in mineral oil) was obtained from Alfa-Aesar and the mineral oil was removed before use. $Mg(NH_2)_2$ was produced in our laboratory by reacting pre-milled Mg power (99%, Sinopharm) with NH_3 (purity 99%) at 300 ºC.[27] Cubic $Li_2MgN_2H_2$ (denoted as *c*-$Li_2MgN_2H_2$) and orthorhombic $Li_2MgN_2H_2$ (denoted as *o*-$Li_2MgN_2H_2$) were synthesised by heating the $Mg(NH_2)_2$-2LiH mixture at different conditions according to equation (3). The detailed synthetic procedure is as follows: a mixture of $Mg(NH_2)_2$ and LiH in a 1:2 molar ratio was transferred into a stainless steel jar and mechanically milled on a planetary ball mill (QM-3SP4, Nanjing) at 500 rpm for 36 h. Afterward, the as-milled mixtures were put into a homemade Sieverts-type apparatus and heated to 280 ºC under dynamic vacuum and 9 bar of hydrogen pressure, respectively. The resultant products were identified as *c*-$Li_2MgN_2H_2$ under dynamic vacuum and *o*-$Li_2MgN_2H_2$ under 9 bar of H_2 (Fig. S1, ESI†).

The two samples ($Mg(NH_2)_2$-2LiH-0.08KF and $Mg(NH_2)_2$-2LiH) were prepared by ball milling the corresponding materials at 500 rpm for 36 h under 50 bar of hydrogen. A gas valve was mounted on the cover of the milling jar and connected to a pressure gauge to measure the internal pressure change before and after ball milling. To prevent contamination by air and water, the samples were handled in a MBRAUN glovebox (Germany) filled with highly pure argon (O_2: < 1 ppm, H_2O: < 1 ppm).

Dehydrogenation/hydrogenation measurements

The dehydrogenation/hydrogenation properties were measured on a homemade Sieverts-type apparatus using the volumetric method. Approximately 120 mg of sample was used in each experiment. In the non-isothermal experiments, the temperature was gradually increased from ambient temperature at 2 ºC/min for dehydrogenation and 1 ºC/min for hydrogenation. For isothermal examination, the samples were quickly heated to and kept at a given temperature during the entire measurement. The reactor was evacuated before the measurements were taken. A primary vacuum (~ 10^{-3} Torr) was applied for dehydrogenation, and the initial hydrogen pressure was 105 bar for hydrogenation. Temperature-dependence of dehydrogenation was examined on a homemade temperature-programmed desorption (TPD) system with an online mass spectrometer (MS) attached which recorded hydrogen (m/z: 2) and ammonia (m/z: 15) simultaneously. About 50 mg of the samples was loaded each time and pure Ar was sent through the sample as the carrier gas in the testing process.

Structural and Morphological Characterisations

The phase structure was characterised with an X'Pert PRO (PANalytical) X-ray diffractometer using Cu Kα radiation at 40 kV and 40 mA. The XRD data were collected in a 2θ range of 10-90º with 0.05º increment steps. To prevent the contamination of the powder samples by air and water, a special container was designed and used during sample transfer and testing.

Infrared measurements were performed using a Bruker Tensor 27 Fourier transform infrared spectrometer (FTIR, Germany) in transmission mode. Powder samples and potassium bromide (KBr) powder in a 1:30 weight ratio were first cold-pressed in the glovebox to form pellets, and the pellets were quickly transferred to the FTIR apparatus for testing. Each spectrum was created using an average of 16 scans with a 4 cm^{-1} resolution. The transfer and testing time was less than 30 s.

The specific surface area (SSA) of the powder samples was determined from N_2 sorption isotherms recorded at 77 K using the Brunauer-Emmett-Teller (BET) method on a Quantachrome Nova 1000e Surface Area and Pore Analyzer (USA). The particle morphologies and sizes of the samples under different conditions were observed with a scanning electron microscope (SEM, Hitachi S4800). The samples were quickly transferred from a glovebox to a SEM facility under a nitrogen atmosphere for protection from air and water. The distribution of elemental K in the samples was detected with an energy-dispersive X-ray spectrometer (EDS) attached to a Hitachi S3400N scanning electron microscope.

Results and discussion

This journal is © The Royal Society of Chemistry [year]

Dehydrogenation/hydrogenation properties of $Mg(NH_2)_2$-2LiH-0.08KF sample

To evaluate the effects of the operating temperature, $Mg(NH_2)_2$-2LiH-0.08KF was first dehydrogenated at 130, 180 and 250 ºC, and the resultant products were subjected to hydrogenation under 105 bar of hydrogen. Fig. 1a shows the dehydrogenation curves for the $Mg(NH_2)_2$-2LiH-0.08KF sample as a function of temperature. For comparison, the dehydrogenation curve of $Mg(NH_2)_2$-2LiH is also presented in Fig. 1a. As reported previously,[26] adding KF significantly decreased the operating temperature for hydrogen release from the $Mg(NH_2)_2$-2LiH system. The $Mg(NH_2)_2$-2LiH-0.08KF sample began to release hydrogen at approximately 80 °C, and the hydrogen release terminated at 210 °C in non-isothermal mode. While the sample was heated to 130 °C and held at this temperature for 48 h, the hydrogen release totalled 5.0 wt% (Fig. S2, ESI†), very similar to the theoretical hydrogen capacity (5.2 wt%). At 180 °C, the total hydrogen released was approximately 5.1 wt%. For dehydrogenation at 250 °C, no additional hydrogen release was observed compared to that at 180 °C. Therefore, almost all available hydrogen in the $Mg(NH_2)_2$-2LiH-0.08KF sample can be released at temperatures as low as 130 °C, revealing significantly improved dehydrogenation properties. Moreover, TPD-MS examinations revealed that the evolution of the side product of NH_3 was also distinctly suppressed with the presence of KF as no NH_3 signal was detected for the KF-added sample in the testing temperature range (Fig. S3, ESI†).[26] It is quite favourable for practical applications.

Fig. 1b shows the hydrogenation curves of the dehydrogenated $Mg(NH_2)_2$-2LiH-0.08KF samples as a function of temperature. Distinct hydrogenation behaviours were observed for these three samples, although they can be completely hydrogenated upon heating to 190 ºC. The sample dehydrogenated at 130 ºC began to take up hydrogen at *ca.* 65 ºC, and approximately 3.5 wt% of hydrogen (70% of hydrogen capacity) was recharged below 130 ºC, exhibiting the superior hydrogenation properties. The sample dehydrogenated at 180 ºC has almost the same onset temperature for hydrogenation as the sample dehydrogenated at 130 ºC. However, the hydrogenation rate of the sample dehydrogenated at 180 °C was slower below 150 ºC compared to the sample dehydrogenated at 130 °C; it could only take up 2.4 wt% of hydrogen at 130 ºC. For the sample dehydrogenated at 250 ºC, the hydrogenation curve shifted distinctly towards higher temperatures, and the onset temperature for hydrogenation increased to 130 ºC; this temperature is 65 °C higher than that of the dehydrogenated samples both at 130 and 180 °C. When increasing the temperature, the hydrogen uptake gradually accelerated, reaching 5.0 wt% while the sample dehydrogenated at 250 °C was heated to 190 °C, similar to the pristine sample. Specifically, the ability of the KF additive to decrease the hydrogenation temperature disappeared after high-temperature dehydrogenation treatments (250 °C).

Further investigations regarding the effects of hydrogenation temperature on the follow-up dehydrogenation were also conducted. First, the as-milled $Mg(NH_2)_2$-2LiH-0.08KF sample was heated to 130 ºC for dehydrogenation. Afterward, the dehydrogenated samples were hydrogenated under 105 bar of hydrogen pressure at 140, 160, 180 and 210 ºC, respectively. Fig. 2 displays the re-dehydrogenation curves of the $Mg(NH_2)_2$-2LiH-0.08KF samples hydrogenated at different temperatures. For comparison, the dehydrogenation curve of the as-milled pristine sample is also shown in Fig. 2. A distinct high-temperature shift in the second dehydrogenation curve of the KF-added sample was observed when increasing the hydrogenation temperature. The sample hydrogenated at 140 ºC began to release hydrogen at only *ca.* 110 ºC, and the midpoint temperature corresponding to half of the dehydrogenation capacity was *ca.* 145 ºC, which is distinctly lower than that of the as-milled pristine sample (*viz.*, $Mg(NH_2)_2$-2LiH). The dehydrogenation behaviour of the sample hydrogenated at 160 ºC is almost identical to that of the sample hydrogenated at 140 °C in addition to the slightly elevated operating temperature and the slightly increased amount of dehydrogenation. After hydrogenation at 180 °C, the onset and midpoint temperatures for the second dehydrogenation were increased to *ca.* 130 and 185 ºC; these temperatures are 20 and 40 ºC higher than those of the previous two samples, respectively. When the hydrogenation temperature was increased to 210 ºC, the onset and midpoint temperatures for hydrogen release were further increased to *ca.* 150 and 207 ºC, which are even higher than those of the as-milled pristine sample. Obviously, elevating the hydrogenation temperature dramatically increases the

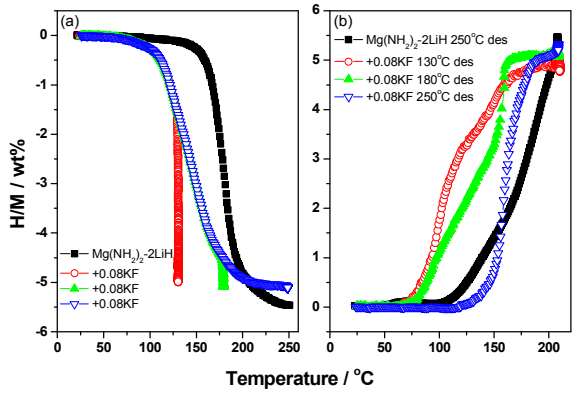

Fig. 1 Dehydrogenation (a) and hydrogenation (b) curves of the $Mg(NH_2)_2$-2LiH and $Mg(NH_2)_2$-2LiH-0.08KF samples.

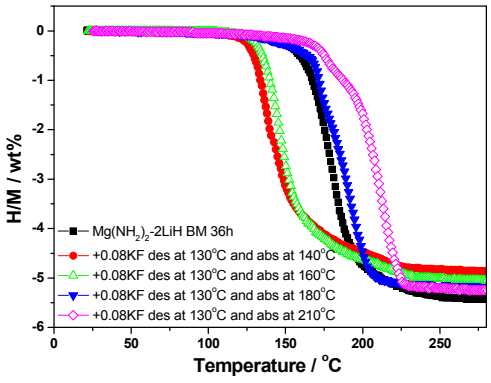

Fig. 2 Re-dehydrogenation curves of the $Mg(NH_2)_2$-2LiH-0.08KF samples hydrogenated at different temperatures (with the as-milled $Mg(NH_2)_2$-2LiH sample for comparison).

operating temperature for the follow-up dehydrogenation. Moreover, the NH_3 signal was also detected again in the dehydrogenation process of the KF-added samples after hydrogenation at higher temperatures. As shown in Fig. S4 (ESI†), the intensities of the NH_3 signal was gradually increased with elevating the hydrogenation temperature. Therefore, the higher operating temperature for the dehydrogenation/hydrogenation of the KF-added $Mg(NH_2)_2$-2LiH sample makes the K-based additive fail during the follow-up hydrogen storage cycling.

Structural and morphology change during dehydrogenation

To understand the underlying reasons for the failure of the K-based additive after high-temperature dehydrogenation, the $Mg(NH_2)_2$-2LiH-0.08KF samples with different treatments were collected and subjected to structural and morphological measurements. Fig. 3 presents the XRD patterns and FTIR spectra of the $Mg(NH_2)_2$-2LiH-0.08KF samples dehydrogenated at 130-250 ºC. As shown in Fig. 3a, the $Mg(NH_2)_2$-2LiH-0.08KF samples dehydrogenated at 130 and 180 ºC exhibit only the characteristic reflection of the cubic $Li_2MgN_2H_2$. For the sample dehydrogenated at 250 °C, the orthorhombic $Li_2MgN_2H_2$ dominates the spectrum due to the absence of the cubic $Li_2MgN_2H_2$ in the XRD profile. Further FTIR examinations display a broad absorbance centred at 3173 cm^{-1} for the samples dehydrogenated at 130 and 180 °C; this signal is ascribed to the typical N-H vibration of the cubic $Li_2MgN_2H_2$.[29] After dehydrogenation at 250 °C, the N-H absorbance centred at 3173 cm^{-1} is invisible and a doublet N-H vibration at 3183/3160 cm^{-1} is observed in the FTIR spectrum, originating from the orthorhombic $Li_2MgN_2H_2$.[30] The $Mg(NH_2)_2$-2LiH-0.08KF samples dehydrogenated at 130 and 180 ºC are mainly composed of the cubic $Li_2MgN_2H_2$, but the composition changes to orthorhombic $Li_2MgN_2H_2$ after dehydrogenation at 250 °C. Specifically, a polymorphic transformation occurs from cubic $Li_2MgN_2H_2$ to orthorhombic $Li_2MgN_2H_2$ at 180-250 °C. For the pristine $Mg(NH_2)_2$-2LiH sample, the dehydrogenation product remains a cubic $Li_2MgN_2H_2$ structure, even at 280 °C (Fig. S1, ESI†).[28] Therefore, we conclude that the presence of the K-based additive in the $Mg(NH_2)_2$-2LiH system induces the polymorphic transformation of the dehydrogenation product (i.e., $Li_2MgN_2H_2$) from cubic structure to orthorhombic structure at elevated

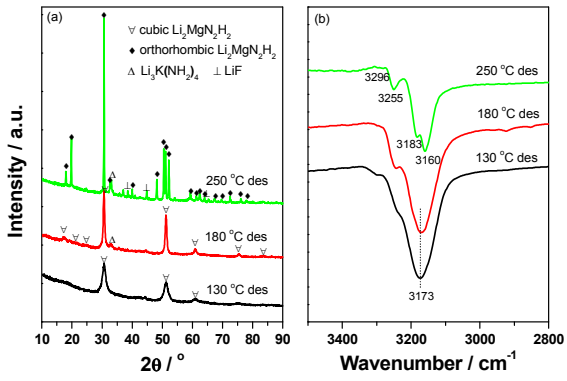

Fig. 3 XRD patterns (a) and FTIR spectra (b) of the $Mg(NH_2)_2$-2LiH-0.08KF samples dehydrogenated at different temperatures.

temperatures. The hydrogenation temperature of the cubic $Li_2MgN_2H_2$ is distinctly lower than that of the orthorhombic sample, as shown in Fig. S5 (ESI†). The onset temperature for the hydrogen uptake of the cubic $Li_2MgN_2H_2$ was approximately only 80 ºC, which is 40 ºC lower than that of the orthorhombic sample (120 ºC). As the temperature was elevated to 180 ºC, the cubic $Li_2MgN_2H_2$ took up approximately 4.0 wt% of hydrogen (~ 80% of hydrogen capacity); however, only 1.4 wt% of hydrogen could be recharged into the orthorhombic sample under the same conditions. Therefore, the hydrogenation properties of $Li_2MgN_2H_2$ have a strong structural dependence. In addition, it should be mentioned that the onset temperature for hydrogenation of the dehydrogenated K-added sample at 250 ºC is higher than that of the dehydrogenated pristine sample as shown in Fig. 1b. This phenomenon can be also reasonably attributed to the occurrence of the polymorphic transformation because the dehydrogenated product of the K-added sample at 250 ºC is the orthorhombic $Li_2MgN_2H_2$ while it is the cubic phase for the dehydrogenated pristine sample. Consequently, we believe that the varied crystal structure of the dehydrogenation product at high operating temperatures is one of the important reasons for the increased hydrogenation temperature of the K-added $Mg(NH_2)_2$-2LiH system during the follow-up cycles, which phenomenologically exhibits the failure of the K-based additive.

Further comparisons of the XRD profiles revealed that the high-temperature dehydrogenation increased crystallisation and enlarged grain sizes for the $Mg(NH_2)_2$-2LiH-0.08KF samples. As shown in Fig. 3a, the broad diffraction peaks were observed in the XRD profile of the dehydrogenated sample at 130 ºC, representing the small grain size, the poor crystallization and/or the amorphous phases. This facilitates the diffusion of hydrogen in the bulk because there is a higher diffusivity of hydrogen either through the amorphous phase or in between the crystalline and amorphous phases.[32] With elevating the dehydrogenation temperature, the diffraction peaks of the dehydrogenation product were distinctly sharpened and intensified, suggesting good crystallisation and an enlarged grain size. According to the Scherrer equation, the grain sizes of $Li_2MgN_2H_2$ were calculated based on the strongest peak (2θ: ~ 30.6º): 10.1, 17.7 and 42.0 nm for the samples dehydrogenated at 130, 180 and 250 °C, respectively. The enlarged grain size reduces the grain boundary and decreases the diffusion path, slowing the diffusivity of the hydrogen through the bulk and possibly inducing slower reaction kinetics for the hydrogenation.

Fig. 4a presents the N_2 sorption isotherms (77 K) of the dehydrogenated $Mg(NH_2)_2$-2LiH-0.08KF samples at 130, 180 and 250 ºC. By using the 6-point BET method, the surface areas were determined to be 58.9, 19.5 and 4.9 $m^2\ g^{-1}$ for the dehydrogenated samples at 130, 180 and 250 ºC, respectively. Apparently, the specific surface area of the samples was gradually decreased with elevating the dehydrogenation temperature. Assuming the sample powders are separated spherical particles, the average particle size can be calculated by the following equation:[33]

$$D=\frac{6}{\rho S} \quad (4)$$

where D is the average particle diameter, ρ is the density, and S is the specific surface area. According to equation (4) and using ρ = 1.18 g cm^{-3} as reported previously,[34] the average particle

This journal is © The Royal Society of Chemistry [year]

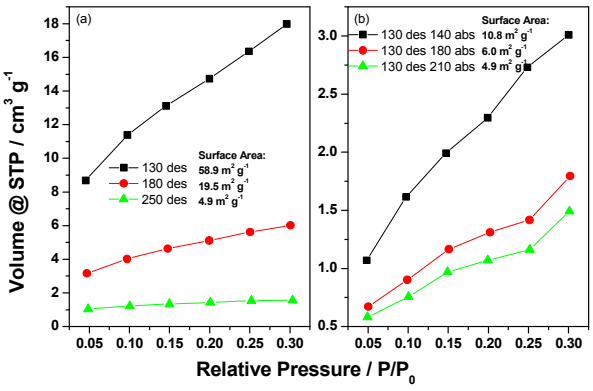

Fig. 4 N_2 sorption isotherms (77 K) of the $Mg(NH_2)_2$-2LiH-0.08KF samples with different treatments.

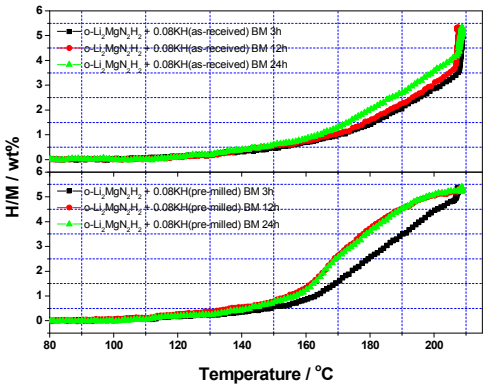

Fig. 5 Hydrogenation curves of the mixtures of orthorhombic $Li_2MgN_2H_2$ with KH.

diameters of the samples dehydrogenated at 130, 180 and 250 ºC were estimated to be *ca.* 86 nm, 261 nm and 1.038 μm. Further SEM observation confirmed such a change in the particle sizes although its distribution is not very uniform (Fig. S6, ESI†). The enlarged particle sizes reduce the specific surface area and lengthen the diffusion distance, increasing the hydrogenation temperature, as shown in Fig. 1b. As reported previously, a > 800 nm $Li_2MgN_2H_2$ sample began to take up hydrogen at 180 ºC; this temperature is approximately 100 ºC higher than that of the 100-200 nm sample,[27] providing quantitative evidence for the effects of the particle size on the hydrogenation properties. Further EDS mapping analyses of the K element showed that after increasing the dehydrogenation temperature, the distribution of the K element changed, becoming somewhat inhomogeneous (Fig. S7, ESI†). A segregation phenomenon occurs with the K element after high-temperature dehydrogenation, likely contributing to the K-based additive failure.

To clarify the effect of the degree of mixing and distribution of the K-based additive on the hydrogenation behaviour of the Li-Mg-N-H system, two series of KH-added $Li_2MgN_2H_2$ samples were designed and prepared because the KF was converted to KH after ball milling treatment.[26] The first was prepared by mixing the as-synthesised orthorhombic $Li_2MgN_2H_2$ and the as-received KH at 100 rpm for 3-24 h. The other was obtained by ball milling the as-received KH at 500 rpm for 36 h and then mixing it with the as-synthesised orthorhombic $Li_2MgN_2H_2$. The two series of $Li_2MgN_2H_2$-0.08KH samples were subjected to hydrogenation under 105 bar of hydrogen as a function of temperature. The results are shown in Fig. 5. For these two sample sets, the hydrogenation temperature was reduced after prolonging the mixing duration, exhibiting identical trends. This phenomenon suggests that the degree of mixing and distribution of the active additive in the matrix critically affects the hydrogenation temperature. In particular, a more distinct decrease in the hydrogenation temperature was observed for the sample with pre-milled KH, indicating that there is a superior effect induced by the degree of mixing and distribution on the small-particle KH. In addition, after being mixed for the same duration, the hydrogenation temperature of the samples with pre-milled KH is significantly lower than that of the samples containing as-received KH, confirming that the particle size of the samples also facilitates changes in the hydrogenation temperature.

Structural and morphology change during hydrogenation

As shown in Fig. 2, the re-dehydrogenation curve of the $Mg(NH_2)_2$-2LiH-0.08KF sample also shifts towards higher temperatures after high-temperature hydrogenation treatments. To obtain detailed structural information, the XRD data of the hydrogenated samples at different temperatures were collected and presented in Fig. 6. All of the hydrogenated samples were primarily composed of three phases: $Mg(NH_2)_2$, LiH and KH. Therefore, the hydrogenation products at 140-210 °C possess identical compositions. However, the samples hydrogenated at 140 and 160 ºC exhibit poor crystallisation; their reflections are very weak and broad. After elevating the hydrogenation temperature, the diffraction peaks of the resultant products are gradually intensified and sharpened, indicating improved crystallisation. A previous report revealed that amorphous $Mg(NH_2)_2$ has higher entropy than that of the well crystallised sample.[14] Therefore, the good crystallisation of the hydrogenation samples at higher temperatures may decrease the entropy change during the dehydrogenation reaction, increasing the thermodynamic barrier and raising the dehydrogenation temperature.

In addition, the grain sizes of the two constituent phases ($Mg(NH_2)_2$ and KH) in the hydrogenated products were calculated according to the Scherrer equation. Table 1 lists the results obtained from the strongest diffraction peak. The elevated hydrogenation temperature enlarges the grain sizes of the constituent phases. As shown in Fig. 6, accurately reading the strongest peak of $Mg(NH_2)_2$ at approximately 30.0º is difficult in the samples hydrogenated at 140 and 160 ºC because this signal is rather broad and weak, suggesting an amorphous state. However, the strongest diffraction peak of KH can be distinguished due to its stronger intensity, particularly for the sample dehydrogenated at 160 °C. The grain sizes of the KH are 13.6 and 14.8 nm for the samples dehydrogenated at 140 and 160 °C, respectively. The small grain size facilitates mass transfer during dehydrogenation due to the increased grain boundary, providing lower operating temperatures during re-dehydrogenation. After hydrogenation at 180 and 210 ºC, the grain sizes of $Mg(NH_2)_2$ were 30.6 and 39.6 nm, respectively, whereas those of KH are 34.1 and 68.2 nm. A

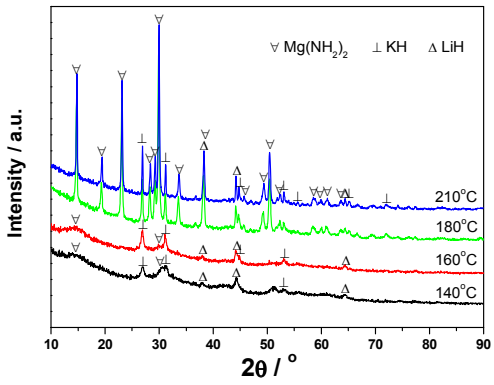

Fig. 6 XRD patterns of $Mg(NH_2)_2$-2LiH-0.08KF hydrogenated at different temperatures.

Table 1 Grain sizes of $Mg(NH_2)_2$ and KH in the hydrogenated $Mg(NH_2)_2$-2LiH-0.08KF samples at different temperatures (unit: nm).

Temperature	$Mg(NH_2)_2$	KH
140 ºC	—	13.6
160 ºC	—	14.8
180 ºC	30.6	34.1
210 ºC	39.6	68.2

distinct increase in the grain size was observed for samples hydrogenated at higher temperatures, increasing the operating temperature of the dehydrogenation/hydrogenation reaction.

The specific surface areas of the hydrogenated samples at different temperatures were also determined with the BET method. The results are shown in Fig. 4b. It is seen that with increasing the hydrogenation temperature, the surface areas of the resultant products are gradually reduced. While hydrogenating at 140 ºC, the surface area of the sample is 10.8 m^2 g^{-1}, and it is reduced to 6.0 and 4.9 m^2 g^{-1} after hydrogenation at 180 and 210 ºC. Correspondingly, the average particle diameters of the samples were calculated to *ca.* 472 nm, 851 nm and 1.045μm. Further SEM observation provides an additional evidence for the enlarged particle sizes as shown in Fig. S8 (ESI†). The increased particle sizes reduce the specific surface area and increase the mass transport lengths for the dehydrogenation reaction, consequently increasing the reaction kinetic barriers and decreasing the diffusion rate. This explains the elevated operating temperature for hydrogen release from the high-temperature hydrogenation product. The apparent activation energy (E_a) and the reaction rate constant (k) were further calculated according to the previous reports.[27,35] As shown in Fig. S9 and S10 (ESI†), the values of E_a and k were determined to be 112 kJ mol^{-1} and 1×10^{-2} s^{-1} for the dehydrogenation reaction of the sample hydrogenated at 140 ºC. After hydrogenation at 180 and 210 ºC, the E_a are increased to 157 and 184 kJ mol^{-1} and the k are decreased to 2.71×10^{-4} and 5.84×10^{-5} s^{-1}, respectively. In other words, the increased hydrogenation temperature significantly slows down the reaction kinetics of the follow-up dehydrogenation.

Moreover, similar to the high-temperature dehydrogenation, a segregation phenomenon of the K element was also observed for the samples after high-temperature hydrogenation, as shown in Fig. S11 (ESI†). The degree of K-based additive distribution correlates closely to the catalytic effect on decreasing the operating temperature for hydrogen storage in $Mg(NH_2)_2$-2LiH.

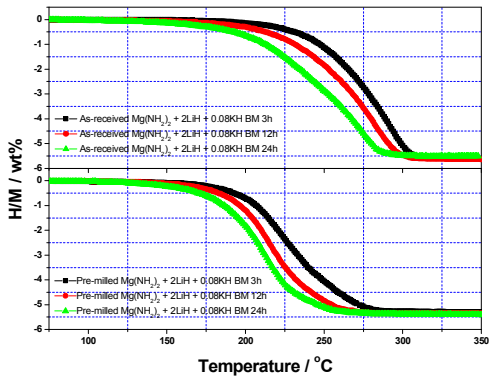

Fig. 7 Dehydrogenation curves of the $Mg(NH_2)_2$-2LiH-0.08KH mixtures after different treatments.

To understand the effect of the particle size and the degree of mixing and distribution of the K-based additive on the dehydrogenation behaviour, as-received and pre-milled $Mg(NH_2)_2$, LiH and KH were employed, and the $Mg(NH_2)_2$-2LiH-0.08KH mixtures were prepared by mixing the corresponding as-received and pre-milled chemicals at 100 rpm. Fig. 7 shows the dehydrogenation curves of the $Mg(NH_2)_2$-2LiH-0.08KH mixtures after different treatments. The dehydrogenation temperature depends on the mixing duration for the samples with and without pre-milling. After prolonged mixing durations, the dehydrogenation temperature gradually decreased, particularly for the pre-milled sample. The degree of mixing and distribution of the K-based additive in the matrix affects the dehydrogenation temperature of the K-added $Mg(NH_2)_2$-2LiH system, and this effect is more distinct for the samples containing small particles. Moreover, compared to the samples without pre-milling, the dehydrogenation temperature of the pre-milled samples is much lower after mixing for the same duration, supporting the effect of particle size on the dehydrogenation temperature of the $Mg(NH_2)_2$-2LiH system. Therefore, the particle size of the sample and the degree of mixing and distribution of the active additive are important for determining the operating temperature for hydrogen storage in the K-added $Mg(NH_2)_2$-2LiH system.

Effects of ball milling on the functional recovery of K-based additive

According to the above discussion, we conclude that the increase in the crystallisation, the enlargement in the grain/particle size of the dehydrogenation/hydrogenation products and the increase in the inhomogeneous degree of mixing and distribution of K-based additive are the three most important reasons for the enhanced operating temperature during the follow-up cycles, phenomenologically representing the failure of the K-based additive, as shown in Fig. 1b and 2. Ball milling is the most common and widely used technique for reducing grain and particle sizes, decreasing the crystallisation and increasing the degree of mixing and distribution of the constituent elements.[31] To confirm our conjecture, the high-temperature dehydrogenation/hydrogenation samples were re-milled on a planetary ball mill at 500 rpm for 36 h. The post-milled products

This journal is © The Royal Society of Chemistry [year]

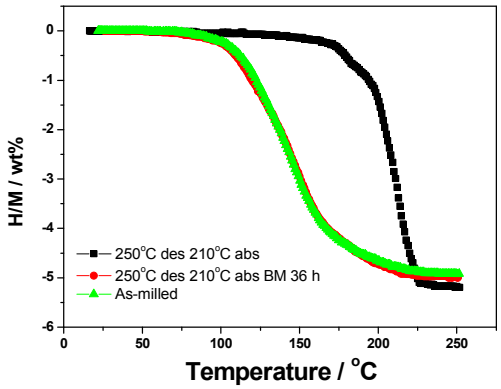

Fig. 8 Dehydrogenation curves of the $Mg(NH_2)_2$-2LiH-0.08KF samples after different treatments.

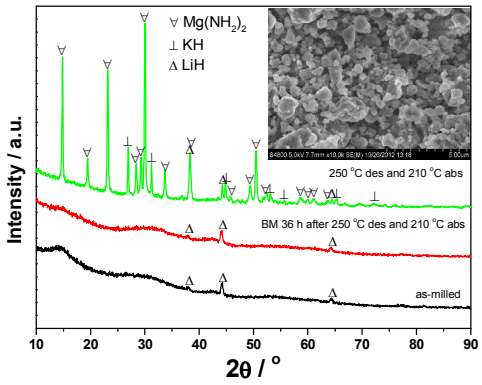

Fig. 9 XRD patterns of the $Mg(NH_2)_2$-2LiH-0.08KF samples after different treatments. The inset is an SEM image of the sample treated first with dehydrogenation/hydrogenation and then ball milling.

were subjected to structural characterisation and property evaluation. Interestingly, the re-dehydrogenation curve of the post-milled high-temperature hydrogenation product moves distinctly towards lower temperatures, overlapping with that of the as-milled sample (Fig. 8). Specifically, the post-milled high-temperature hydrogenation product exhibits dehydrogenation behaviour identical to that of the as-milled sample, indicating that the ability of the K-based additive to improve the hydrogen storage properties of the $Mg(NH_2)_2$-2LiH sample are recovered.

Fig. 9 presents the XRD patterns of the $Mg(NH_2)_2$-2LiH-0.08KF samples after different treatments. The $Mg(NH_2)_2$-2LiH-0.08KF sample dehydrogenated at 250 ºC and then hydrogenated at 210 ºC exhibits very sharp reflections with considerable intensities in the XRD profile, signifying good crystallisation. However, after ball milling for 36 h at 500 rpm, the diffraction peaks of the sample were distinctly broadened and weakened, suggesting poor crystallisation and reduced grain size. In addition, the XRD pattern is very similar to that of the as-milled sample, revealing their identical structural characteristics. Further SEM observations display significantly reduced particle sizes for the post-milled hydrogenation products (the inset of Fig. 9). As mentioned above, the particle size of the sample hydrogenated at 210 ºC is above 1 μm (Fig. S8, ESI†). After ball milling treatment, the particle size is roughly reduced to 0.2-0.5 μm, in addition to a small number of coarse particles, similar to the as-milled sample shown in Fig. S12 (ESI†). Obviously, the structure and morphology of the high-temperature hydrogenation product are recovered, reaching the initial state after ball milling and re-activating the K-based additive. Consequently, we believe that the failure of the K-based additive after high-temperature treatments should only be phenomenological instead of natural. After ball milling, the ability of the K-based additive to lower the operating temperature for hydrogen storage in the $Mg(NH_2)_2$-2LiH system can be completely recovered. Therefore, strictly controlling the dehydrogenation/hydrogenation of the K-added $Mg(NH_2)_2$-2LiH system at lower temperatures is crucial for maintaining the superior effect of the K-based additive.

Conclusions

In this paper, a high-temperature failure mechanism for K-based additives meant to improve the hydrogen storage properties of a $Mg(NH_2)_2$-2LiH system was systematically investigated and elucidated using a series of structural and morphological characterisations. First, a polymorphic transformation was observed, changing the cubic structure to an orthorhombic structure for the resultant product (*i.e.*, $Li_2MgN_2H_2$) in the KF-added $Mg(NH_2)_2$-2LiH sample after high-temperature dehydrogenation (> 180 °C). However, the dehydrogenation product remained a cubic $Li_2MgN_2H_2$ structure, even at 280 °C, for the pristine $Mg(NH_2)_2$-2LiH sample. Further comparisons revealed that the hydrogenation temperature of the orthorhombic $Li_2MgN_2H_2$ was distinctly higher than that of the cubic sample. Second, the grain/particle sizes of the dehydrogenated/hydrogenated $Mg(NH_2)_2$-2LiH-0.08KF samples at higher temperatures were much larger than that of the resultant products at lower temperatures. The enlarged grains reduce the grain boundary and decrease the diffusion path, hindering the diffusivity of the hydrogen through the bulk. In addition, the enlarged particle size reduces the specific surface area and increases the mass transport lengths for the dehydrogenation reaction. Third, there is a segregation phenomenon for the K element after high-temperature dehydrogenation/hydrogenation treatments, inducing an inhomogeneous distribution of K element and reducing the catalytic activity of the K-based additive. These three factors are the most important reasons for the enhanced operating temperature in the following cycles after high-temperature dehydrogenation/hydrogenation treatment. More interestingly, the ability of the K-based additive to improve the hydrogen storage properties of the $Mg(NH_2)_2$-2LiH sample were recovered after energetic ball milling the high-temperature dehydrogenation/hydrogenation samples. The high-temperature dehydrogenation/hydrogenation product milled at 500 rpm for 36 h exhibited dehydrogenation behaviours identical to the freshly milled sample due to the decreased crystallisation, reduced grain/particle size and improved mixing and distribution degree of the constituent species. We believe that the failure of K-based additive after high-temperature treatment is only phenomenological rather than natural.

Acknowledgements

The authors would like to acknowledge the financial support from the Ministry of Science and Technology of China (2010CB631304), the National Natural Science Foundation of China (51222101, 51025102, 51171170), the Research Fund for the Doctoral Program of Higher Education of China (20130101110080, 20130101130007), the Program for Innovative Research Team in University of Ministry of Education of China (IRT13037), and the Science and Technology Department of Zhejiang Province (2010R50013).

Notes and references

State Key Laboratory of Silicon Materials, Key Laboratory of Advanced Materials and Applications for Batteries of Zhejiang Province and Department of Materials Science and Engineering, Zhejiang University, Hangzhou 310027, China. Tel/Fax: +86 571 87952615; E-mail: mselyf@zju.edu.cn (Y.F.L.) hgpan@zju.edu.cn (H.G.P.)

† Electronic Supplementary Information (ESI) available: [XRD and FTIR data for the as-prepared $Li_2MgN_2H_2$, dehydrogenation curves for the $Mg(NH_2)_2$-2LiH-0.08KF sample as a function of time and temperature, MS of the samples with and without KF, hydrogenation curves for the cubic and orthorhombic $Li_2MgN_2H_2$, SEM images and EDS maps of K for the dehydrogenated KF-added samples, Kissinger's plots, isothermal dehydrogenation curves and the corresponding Ginstling-Brounshtein's plots of the KF-added samples, SEM images and EDS maps of K for the hydrogenated KF-added samples, SEM images of the post-milled KF-added sample after cycling]. See DOI: 10.1039/b000000x/

1 L. Schlapbach and A. Züttel, *Nature*, 2001, **414**, 353.
2 P. Chen, Z. T. Xiong, J. Z. Luo, J. Y. Lin and K. L. Tan, *Nature*, 2002, **420**, 302.
3 P. Chen, Z. T. Xiong, G. T. Wu, Y. F. Liu, J. J. Hu and W. F. Luo, *Scrip. Mater.*, 2007, **56**, 817.
4 Z. T. Xiong, G. T. Wu, H. J. Hu and P. Chen, *Adv. Mater.*, 2004, **16**, 1522.
5 W. F. Luo, *J. Alloys Compd.*, 2004, **381**, 284.
6 Z. T. Xiong, J. J. Hu, G. T. Wu, P. Chen, W. F. Luo, K. Gross and J. Wang, *J. Alloys Compd.*, 2005, **398**, 235.
7 A. Sudik, J. Yang, D. Halliday and C. Wolverton, *J. Phys. Chem. C*, 2007, **111**, 6568.
8 Y. Chen, P. Wang, C. Liu and H.-M. Cheng, *Int. J. Hydrogen Energy*, 2007, **32**, 1262.
9 W. Lohstroh and M. Fichtner, *J. Alloys Compd.*, 2007, **446**, 332.
10 R. R. Shahi, T. P. Yadav, M. A. Shaz and O. N. Srivastva, *Int. J. Hydrogen Energy*, 2010, **35**, 238.
11 J. C. Wang, Z. N. Li, H. L. Li, J. Mi, F. Lu, S. M. Wang, X. P. Liu and L. J. Jiang, *Rare Metals*, 2010, **29**, 621.
12 L. P. Ma, P. Wang, H. B. Dai and H. M. Cheng, *J. Alloys Compd.*, 2009, **468**, L21.
13 L. P. Ma, Z. Z. Fang, H. B. Dai, X. D. Kang, Y. Liang, P. J. Wang, P. Wang and H. M. Cheng, *J. Mater. Res.*, 2009, **24**, 1936.
14 J. H. Wang, J. J. Hu, Y. F. Liu, Z. T. Xiong, G. T. Wu, H. G. Pan and P. Chen, *J. Mater. Chem.*, 2009, **19**, 2141.
15 L. P. Ma, H. B. Dai, Y. Liang, X. D. Kang, Z. Z. Fang, P. J. Wang, P. Wang and H. M. Cheng, *J. Phys. Chem. C*, 2008, **112**, 18280.
16 C. Liang, Y. F. Liu, Z. J. Wei, Y. J. Jiang, F. Wu, M. X. Gao and H. G. Pan, *Int. J. Hydrogen Energy*, 2011, **36**, 2137.
17 J. J. Hu, Y. F. Liu, G. T. Wu, Z. T. Xiong, Y. S. Chua and P. Chen, *Chem. Mater.*, 2008, **20**, 4398.
18 J. J. Hu, A. Pohl, S. M. Wang, J. Rothe and M. Fichtner, *J. Phys. Chem. C*, 2012, **116**, 20246.
19 C. Liang, Y. F. Liu, Y. Jiang, Z. J. Wei, M. X. Gao, H. G. Pan and Q. D. Wang, *Phys. Chem. Chem. Phys.*, 2011, **13**, 314.
20 H. G. Pan, S. B. Shi, Y. F. Liu, B. Li, Y. J. Yang and M. X. Gao, *Dalton Trans.*, 2013, **42**, 3802.
21 B. Li, Y. F. Liu, J. Gu, M. X. Gao and H. G. Pan, *Chem. Asian J.*, 2013, **8**, 374.
22 J. H. Wang, T. Liu, G. T. Wu, W. Li, Y. F. Liu, C. M. Araujo, R. H. Scheicher, A. Blomqvist, R. Ahuja, Z. T. Xiong, P. Yang, M. X. Gao, H. G. Pan and P. Chen, *Angew. Chem. Int. Ed.*, 2009, **48**, 5828.
23 T. Durojaiye and A. Goudy, *Int. J. Hydrogen Energy*, 2012, **37**, 3298.
24 W. Luo, V. Stavila and L. E. Klebanoff, *Int. J. Hydrogen Energy*, 2012, **37**, 6646.
25 C. Liang, Y. F. Liu, M. X. Gao and H. G. Pan, *J. Mater. Chem. A*, 2013, **1**, 5031.
26 Y. F. Liu, C. Li, B. Li, M. X. Gao and H. G. Pan, *J. Phys. Chem. C*, 2013, **117**, 866.
27. Y. F. Liu, K. Zhong, K. Luo, M. X. Gao, H. G. Pan and Q. D. Wang, *J. Am. Chem. Soc.*, 2009, **131**, 1862.
28 C. Li, Y. F. Liu, Y. J. Gu, M. X. Gao and H. G. Pan, *Chem. Asian J.*, 2013, **8**, 2136.
29 J. J. Hu, Y. F. Liu, G. T. Wu, Z. T. Xiong and P. Chen, *J. Phys. Chem. C*, 2007, **111**, 18439.
30 T. Markmaitree and L. L. Shaw. *J. Power Sources*, 2010, **195**, 1984.
31 V. Berube, G. Radtke, M. Dresselhaus and G. Chen, *Int. J. Energy Res.*, 2007, **31**, 637.
32 N. H. Goo and K. S. Lee, *Int. J. Hydrogen Energy*, 2002, **27**, 433.
33 A. C. Dodd, A. J. McKinley, M. Saunders and T. Tsuzuki, *J. Nanopart. Res.* 2006, **8**, 43.
34 R. Janot, J. B. Eymery and J. M. Tarascon, *J. Power Sources*, 2007, **164**, 496.
35 H. E. Kissinger, *Anal. Chem.* 1957, **29**, 1702.

This journal is © The Royal Society of Chemistry [year]